IOP PUBLISHING JOURNAL OF PHYSICS A: MATHEMATICAL AND THEORETICAL

J. Phys. A: Math. Theor. **41** (2008) 304026 (19pp) doi:10.1088/1751-8113/41/30/304026

Linear transformations and aberrations in continuous and finite systems

Kurt Bernardo Wolf

Instituto de Ciencias Físicas, Universidad Nacional Autónoma de México, Av. Universidad s/n, Cuernavaca, Morelos 62251, Mexico

E-mail: bwolf@fis.unam.mx

Received 30 November 2007, in final form 13 March 2008
Published 15 July 2008
Online at stacks.iop.org/JPhysA/41/304026

Abstract

In geometric optics there is a natural distinction between the paraxial and aberration regimes, which contain respectively the linear and nonlinear canonical transformations of position and momentum in the phase space. In the Lie-theoretical presentation, linear inhomogeneous transformations are generated by linear and quadratic functions of the phase space, while aberrations of increasing order are generated by homogeneous functions with higher powers of these coordinates. In a way parallel but distinct from the Schrödinger quantization of continuous classical systems, we quantize the geometric optical model into discrete, finite-dimensional systems based on the Lie algebra $\mathsf{su}(2)$, whose wavefunctions are N-point signals, phase space is a sphere and transformations are represented by the $N \times N$ unitary matrices that form the group $\mathsf{U}(N)$. We factor this group into $\mathsf{SU}(2)$-linear and nonlinear unitary transformations of phase space and classify all its $N^2 - 4$ aberrations. This offers a new parametrization of $\mathsf{U}(N)$ based on a chosen $\mathsf{SU}(2)$ subgroup.

PACS numbers: 02.20.Qs, 42.15.Fr

1. Introduction

We are interested in describing the unitary transformations that can be performed on an N-point signal, in particular when these transformations are modeled after geometric optical systems whose paraxial action and aberrations are known [1, part 4]. Here we propose a classification for the aberrations of finite systems as due to evolution by a basis of monomials in the classical phase-space coordinates. These aberrations will respect conservation laws and belong to the group $\mathsf{U}(N)$ of all $N \times N$ unitary matrices.

The analysis of finite systems can be made from several viewpoints and various purposes. The fast Fourier transform algorithm (FFT) has provided an efficient way of computing results and is thus favored for actual applications; the concomitant description of periodic signals

is on a phase-space torus [2, 3], which has led to many proposals for non-standard quantum dynamics [4, 5]. Another avenue of research on the phase-space representation for periodic signals is contained in the works of Opatrný [6, 7] and of Alonso, Forbes *et al* [8–10], where uncertainty measures are found which obey the complementarity principle for Fourier series and finite Fourier transforms.

One obstacle to applying some of these models to optical parallel processors has been the difficulty in establishing what a 'paraxial régime' is—including the (not unique) definition of a one-parameter group of finite-dimensional *fractional* Fourier transform matrices [11, chapter 6]. This problem has been cut down computationally by Koç, Ozaktas *et al* [12] by sampling the continuum definition and appropriately factoring all linear canonical transformations into chirp, scaling and the FFT, so that the computational complexity remains $\sim N \log_2 N$. Still, it is fair to say that the processing of wavefields, sampled into finite signals, has remained paraxial. Aberrations, understood as nonlinear canonical transformations of phase space, have not been treated on a similar footing.

Our approach to representing finite signals and their transformations has been group-theoretical, both in the classical model of geometric optics [1] and in the present $\mathsf{su}(2)$ model for finite systems. Instead of quantizing a classical system *á la Schrödinger* through the Heisenberg commutator of position and momentum operators, we use the Lie algebra $\mathsf{su}(2)$ to define their *finite quantization* to $N \times N$ Hermitian matrices. The generators of $\mathsf{su}(2)$, commonly associated with angular momentum and spin, are given new roles: they will stand for the position, momentum and the (displaced) energy of a harmonic oscillator [13, 14]; thus they will naturally have N equally-spaced eigenvalues. Finite quantization also entails a 'meta-phase space' whose coordinates are these three variables [15]. When the number of points N is fixed, this space can be reduced to the 2-sphere in R^3 [16], with a Wigner quasi-probability distribution function that shows these signals and serves to interpret their transformations in a semiclassical way as flows on the sphere. Linear transformations are rigid $\mathsf{su}(2)$ rotations of the sphere [17], while nonlinear transformations of this manifold are its aberrations [18, 19].

In section 2 we give the geometric optical model, recalling the classification of linear transformations and Hamilton–Lie aberrations; these provide the factored-product parametrization of the canonical transformations of the phase space. A similar approach is taken in section 3 on a three-dimensional space whose commuting variables satisfy $\mathsf{su}(2)$ under Poisson-like brackets. In section 4 we provide the $\mathsf{su}(2)$ model for N-point finite systems and their linear transformations based on the geometric model of the previous section; here, the phase space is a sphere. $\mathsf{su}(2)$ aberrations are introduced and studied in sections 5 and 6; they are elements of the cover algebra $\overline{\mathsf{su}}(2)$ in an $N \times N$ Hermitian matrix representation, and generate the group $\mathsf{U}(N)$ of all unitary signal transformations. To see how these transformations act on signals we must briefly recall the $\mathsf{su}(2)$ Wigner function on the sphere in section 7, which is further detailed in the appendix. With these tools we show the first few aberrations of a rectangle signal in section 8 and offer some conclusions and matters for further research in section 9.

2. Canonical maps of the phase plane

In plane geometric optics, with the phase-space coordinates of position and momentum $(q, p) \in \mathsf{R}^2$, one introduces the basic Poisson bracket $\{q, p\}_{\text{Pb}} = 1$, and defines those transformations that preserve it as canonical. For instance, translations are generated by the Poisson operator of momentum $\{p, \circ\}_{\text{Pb}} = -\partial_q$ through its Lie exponential, whose canonical

action on functions of the phase-space coordinates is

$$\exp(\alpha\{p,\,\circ\}_{\rm Pb}) : f(q,\,p) = f(q-\alpha p,\,p). \tag{1}$$

Generally, inhomogeneous linear transformations of phase space are generated by the Poisson operators of functions that are linear and quadratic in these variables respectively, exponentiated into the operators of translation and linear action,

$$\mathcal{T}(v_1,\,v_2) := \exp\{v_1 q + v_2 p,\,\circ\}_{\rm Pb}, \tag{2}$$

$$\mathcal{L}(u_1,\,u_2,\,u_3) := \exp\{u_1 q^2 + u_2 qp + u_3 p^2,\,\circ\}_{\rm Pb}. \tag{3}$$

In particular, the Poisson operator of $\frac{1}{2}p^2$ generates (Fresnel) free flight, pq generates squeezing, $\frac{1}{2}q^2$ a thin (Fresnel) lens, and the motion in a harmonic waveguide is generated by the classical oscillator Hamiltonian,

$$h^{\rm osc}(q,\,p) := \tfrac{1}{2}(p^2+q^2). \tag{4}$$

Beyond quadratic functions, $\{f(q,\,p),\,\circ\}_{\rm Pb}$ will generate nonlinear transformations of the $(q,\,p)$-plane—aberrations—that conserve Poisson brackets and are thus canonical [20], and whose lines of flow on phase space $(q,\,p) \in \mathsf{R}^2$ are $f(q,\,p) =$ constant. In [21], [1, part 4] aberrations were classified by the basis of monomial functions

$$M_{k,m}(q,\,p) := q^{k-m}\,p^{k+m} \quad \begin{cases} \text{for } \textit{rank} & k \in \{0,\,\tfrac{1}{2},\,1,\,\tfrac{3}{2},\,\dots\}, \\ \text{and } \textit{weight} & m \in \{k,\,k-1,\,\dots,\,-k\}. \end{cases} \tag{5}$$

When $k = \frac{1}{2}$ and 1, the Poisson operators $\{M_{k,m},\,\circ\}_{\rm Pb}$ generate the translations and linear transformations in (2) and (3). For $k > 1$ they generate nonlinear transformations—aberrations—of integer order $A = 2k - 1 \geqslant 2$.

In figure 1, we show the linear action and aberrations on a patch of phase space generated by each of the (Poisson operators of the) monomials $M_{k,m}(q,\,p)$ in (5). As noted above, the lines of flow in these aberrations are $M_{k,m}(q,\,p) =$ constant, as shown in figure 2 for the $A = 3$ $(k = 2)$ quintuplet of aberrations. Except for the straight lines when $m = \pm k$, the lines of flow are like hyperbolas, with different asymptotic powers and directions of flow. Some of these aberrations correspond closely to the traditional Seidel nomenclature: all $m = k$ monomials generate spherical aberrations (of orders $A = 2k - 1$), $m = k - 1$ generate the comas, $m = -k + 1$ the distortions and $m = -k$ the pocuses [21].

The factored product order parametrization proposed by Dragt *et al* [22, 23] for geometric optical canonical transformations on the two-dimensional phase space is based on the monomials (5); this is the $k \to \infty$ limit of

$$\mathcal{C}(\mathbf{A}) = \exp\left(\sum_{m=-k}^{k} A_{k,m}\{M_{k,m},\,\circ\}_{\rm Pb}\right) \times \cdots \tag{6}$$

$$\times \exp\Big(\sum_{m=-3/2}^{3/2} A_{\frac{3}{2},m}\{M_{\frac{3}{2},m},\,\circ\}_{\rm Pb}\Big) \tag{7}$$

$$\times\, \mathcal{L}(A_{1,-1},\,A_{1,0},\,A_{1,1}) \tag{8}$$

$$=: \prod_{\kappa=k}^{1}{}^{>} \exp(\mathbf{A}_{\kappa,\cdot} \cdot \{\mathbf{M}_{\kappa,\cdot},\,\circ\}_{\rm Pb}), \tag{9}$$

where (8) are the three linear transformations in (3), (6)–(7) are the $2k^2+3k-5 = \frac{1}{2}A^2+\frac{5}{2}A-3$ aberrations, and in (9) the symbol $\Pi_{\kappa}^{>}$ orders the factors by decreasing values of κ from k to 1 in

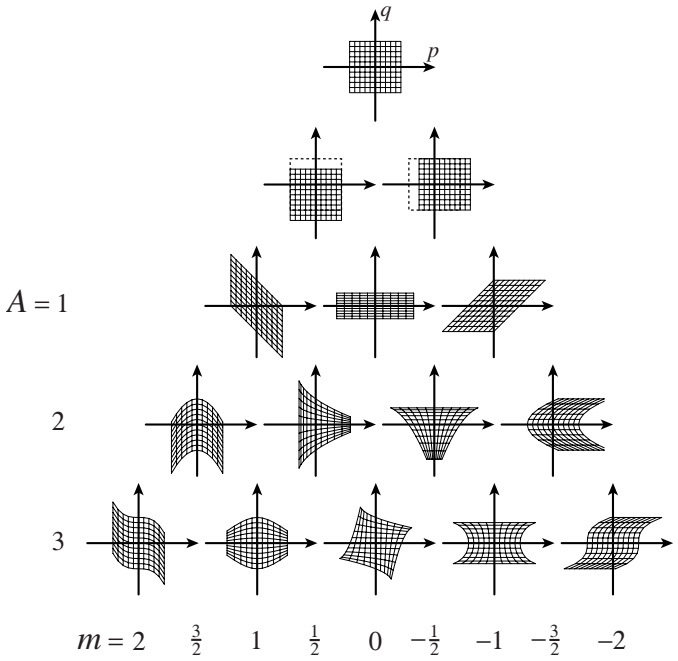

Figure 1. Monomial aberrations of the two-dimensional classical phase-space plane $(q, p) \in \mathsf{R}^2$, classified by aberration order $A = 2k-1$ (rank k) and weight m ($|m| \leqslant k$). At $k = 0$ is the unit map; the two translations (2) have rank $k = \frac{1}{2}$ ($A = 0$); the three linear transformations (3) have rank $k = 1$ ($A = 1$). Nonlinear canonical transformations are shown for aberration orders $A = 2, 3$ ($k = \frac{3}{2}, 2$).

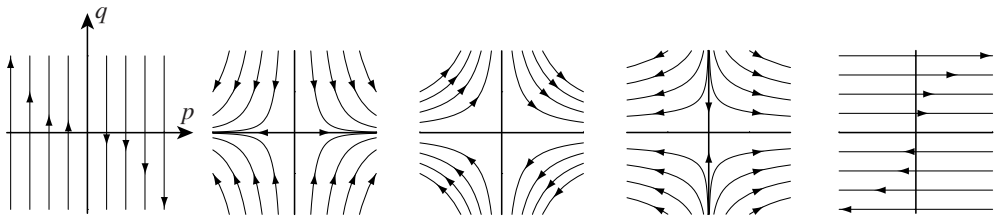

Figure 2. Lines of flow in the five third-order aberrations of the previous figure (rank $k = 2$, $A = 3$). From left to right: weights $m = 2, 1, 0, -1, -2$ (spherical aberration, coma, astigmatism curvature of field, distortion, pocus).

steps of $\frac{1}{2}$. One can consistently truncate the aberration order and thus have a finite-parameter group of transformations. The aberration coefficients can be organized as a list of lists,

$$\mathbf{A} \equiv \{\mathbf{A}_\kappa\}_{\kappa=1}^{k} \equiv \left\{\{A_{\kappa,m}\}_{m=-\kappa}^{\kappa}\right\}_{\kappa=1}^{k}, \tag{10}$$

which are available for axis-symmetric systems (where only odd aberration orders appear), such as free flight, centered polynomial-profile refracting surfaces and anharmonic waveguides [1, chapter 13], complemented by their concatenation product law, for aberration orders up to seven.

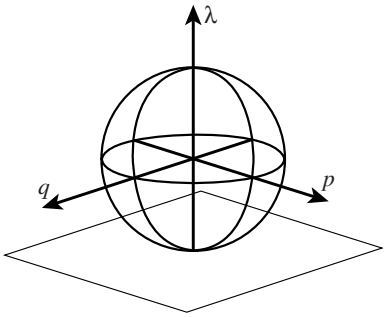

Figure 3. The sphere (13) in the classical meta-phase space $(q, p, \lambda) \in \mathsf{R}^3$, with Cartesian axes of position q, momentum p, and (displaced) energy λ. At the 'bottom pole' $\lambda \approx -r$ the tangent (q, p)-plane is the phase space of paraxial geometric optics.

3. Canonical maps on the classical sphere

Now consider a classical system with three real observables, $(q, p, \lambda) \in \mathsf{R}^3$, that we call *position*, *momentum* and *energy* (whose zero value can be adjusted). We let these three quantities satisfy the $\mathsf{su}(2)$ Berezin brackets:

$$\{\lambda, q\}_{\mathrm{B}} = p, \qquad \{p, \lambda\}_{\mathrm{B}} = q, \qquad \{q, p\}_{\mathrm{B}} = \lambda. \tag{11}$$

Berezin brackets can be realized by differential operators with the same properties as Poisson brackets. The first and second brackets in (11) are the geometric and dynamic Hamilton equations for the harmonic oscillator, with $h = \lambda +$ constant being the Hamiltonian. The third bracket—between position and momentum—is non-standard; it determines the $\mathsf{su}(2)$ finite oscillator model [14], which is well known under the guise of quantum angular momentum theory [24].

Linear functions of q, p, λ generate the $\mathsf{SU}(2)$ Lie group of operators

$$R(\mathbf{v}) := \exp\{v_1 q + v_2 p + v_3 \lambda, \circ\}_{\mathrm{B}}, \tag{12}$$

which in the three-dimensional space of Cartesian coordinates (q, p, λ) produce rigid rotations of all spheres

$$q^2 + p^2 + \lambda^2 = r^2, \tag{13}$$

of radius r, shown in figure 3. We call these transformations $\mathsf{SU}(2)$-*linear*, and refer to $(q, p, \lambda) \in \mathsf{R}^3$ as the $\mathsf{su}(2)$ *meta-phase* space.

Non-rigid transformations of sphere (13) are generated by nonlinear differentiable functions $f(q, p, \lambda)$ through their exponentiated Berezin operators

$$S_f(\alpha) := \exp(\alpha\{f(q, p, \lambda), \circ\}_{\mathrm{B}}). \tag{14}$$

Such transformations preserve the Berezin brackets (11), and will be said to be $\mathsf{SU}(2)$-*canonical*; a basis for these is the monomials $\{q^a p^b \lambda^c, \circ\}_{\mathrm{B}}$, which form under commutation the infinite-dimensional Lie algebra $\overline{\mathsf{su}}(2)$. The flow lines of the meta-phase space under (14) are the intersection of the spheres $r =$ constant with the family of surfaces $f(q, p, \lambda) =$ constant.

Following the rather evident classification of the monomials (5) into multiplets of $2k + 1$ aberrations for each rank $k \in \{0, \frac{1}{2}, 1, \ldots\}$, and being aware that the powers of λ will be curtailed on the sphere by (13) to be 0 or 1, we propose the following linearly independent monomials, labeled by m, to generate the $\mathsf{su}(2)$ aberrations of orders $A = 2k$,

$$M^0_{k,m}(q,\,p) := p^{k+m}q^{k-m}, \qquad m \in \{-k,\,-k{+}1,\,\ldots,\,k\}, \tag{15}$$

$$M^1_{k,m}(q,\,p,\,\lambda) := \lambda M^0_{k-1/2,m}(q,\,p), \qquad m \in \left\{-k{+}\tfrac{1}{2},\,-k{+}\tfrac{3}{2},\,\ldots,\,k{-}\tfrac{1}{2}\right\}. \tag{16}$$

The generic appearance of the flow lines generated by these monomials on the sphere should coincide, within a neighborhood of the bottom pole of figure 3, with the flow of figure 2. The flows of the generic $M^0_{k,\pm k}$ aberrations wring the sphere along $p =$ constant and $q =$ constant circles respectively; for $-k < m < k$, both the maximal circles $q = 0$ and $p = 0$ are lines that divide the sphere into four quadrants whose flows do not mix. The difference between $M^0_{k,m}(q,\,p)$ in (15) and $M^1_{k,m}(q,\,p,\,\lambda)$ in (16) lies in the fact that the latter divide the flow into octants of the sphere, since the $\lambda = 0$ maximal circle is now also a line of flow. In a neighborhood of the top pole of figure 3 therefore, the flows on the sphere will be opposite to those on the bottom pole.

In the plane case with Poisson brackets $\{q,\ p\}_{\text{Pb}} = 1$, the aberration order of the generator $\{M_{k,m},\ \circ\}_{\text{Pb}}$ is counted by $A^{\text{Pb}} = 2k - 1$, because on the phase space the leading nonlinear term in the exponential series (6), $\{M_{k,m},\ w\}_{\text{Pb}}$ $(w = q,\,p)$, is of polynomial degree $2k - 1$. On the sphere with Berezin brackets however, the leading term of the exponential series of $\left\{M^\sigma_{k,m},\ w\right\}_{\text{B}}$ $(w = q,\,p,\,\lambda)$ is of degree $A \equiv A^{\text{B}} = 2k$; because the su(2) algebra is semisimple, the degree is not reduced.

The classical su(2) model on the sphere described in this section is a deformation of the geometric optical model on the plane revised in section 2. The former contracts to the latter when the radius r of the sphere grows without bound. To show this, consider a neighborhood of the bottom pole of the sphere ($\lambda = h - r$ with h finite), and introduce the scaled variables $\bar q := q/\sqrt{r}$, $\bar p := p/\sqrt{r}$ that satisfy $\{\bar q,\ \bar p\}_{\text{B}} = 1$; when $r \to \infty$ the two standard brackets in (11) remain as the classical harmonic oscillator equations, with the limiting Hamiltonian function $h = \frac{1}{2}(\bar p^2 + \bar q^2)$.

4. Finite *N*-point systems

The classification of linear transformations and aberrations on the sphere generated by the basis of monomials (15)–(16) is the su(2) analog of the classification (5) for geometric optics with Poisson brackets [21]. The classical model on the sphere will be now 'su(2)-quantized' into a finite system, and represented by finite matrices acting on column vectors.

The su(2) model for finite systems of $N = 2j + 1$ points postulates that the three observables q, p, λ of the previous section are the spectra of the three generators of this algebra, abstractly denoted by $\mathcal{L}_1$, $\mathcal{L}_2$, $\mathcal{L}_3$, with the su(2) commutation relations $[\mathcal{L}_k,\,\mathcal{L}_l] = \mathrm{i}\varepsilon_{k,l,m}\mathcal{L}_m$ $(k, l, m$ cyclic)—the same structure of (11), in a unitary irreducible representation j of this algebra. Their correspondence with the physical observables will be:

$$\text{position:} \qquad \mathcal{Q} = \mathcal{L}_1, \tag{17}$$

$$\text{momentum:} \qquad \mathcal{P} = \mathcal{L}_2. \tag{18}$$

$$\text{energy:} \qquad \mathcal{H} = \mathcal{L}_3 + \left(j{+}\tfrac{1}{2}\right)I, \tag{19}$$

where I is the unit operator that enlarges su(2) to u(2) = u(1) $\oplus$ su(2). The 'physical' commutation relations characterizing this model are thus:

$$[\mathcal{H},\,\mathcal{Q}] = \mathrm{i}\mathcal{P}, \qquad [\mathcal{P},\,\mathcal{H}] = \mathrm{i}\mathcal{Q}, \qquad [\mathcal{Q},\,\mathcal{P}] = \mathrm{i}\left[\mathcal{H} - \left(j{+}\tfrac{1}{2}\right)I\right], \tag{20}$$

as in (11), but now the abstract generators act on N-point complex signals ($N = 2j{+}1$) as $N \times N$ matrices. Let us agree to call $\mathcal{L} \equiv \mathcal{L}_3 = \mathcal{H} - \big(j{+}\frac{1}{2}\big)I$. In this representation, the Casimir operator is a multiple of the identity,

$$\mathcal{Q}^2 + \mathcal{P}^2 + \mathcal{L}^2 = j(j{+}1)I. \tag{21}$$

It follows from the theory of quantum angular momentum that the spectra of position $\{q\}$, momentum $\{p\}$ and (displaced) energy $\{\lambda\}$ are real, and intrinsically discrete, finite and equally spaced: $q, p, \lambda \in \{-j, -j{+}1, \ldots, j\}$. But while in angular momentum theory $\mathcal{L} \equiv \mathcal{L}_3$ is commonly represented by a diagonal matrix (classifying the $2j{+}1$ states of the multiplet by their 'magnetic' quantum number), in the su(2) model the signal points are numbered in the eigenbasis of position $\mathcal{Q}$, so that here $\mathcal{L}_1$ will be diagonal.

Denote the matrix representations of $\mathcal{Q}, \mathcal{P}$ and $\mathcal{L}$ in (17)–(19) by $\mathbf{Q} = \|Q_{q,q'}\|, \mathbf{P} = \|P_{q,q'}\|$ and $\mathbf{L} = \|L_{q,q'}\|$, with the elements

$$Q_{q,q'} = q\delta_{q,q'}, \qquad q, q' \in \{-j, -j{+}1, \ldots, j\}, \tag{22}$$

$$P_{q,q'} = -\mathrm{i}\big(\tfrac{1}{2}\sqrt{(j{-}q)(j{+}q{+}1)}\delta_{q+1,q'} - \tfrac{1}{2}\sqrt{(j{+}q)(j{-}q{+}1)}\delta_{q-1,q'}\big), \tag{23}$$

$$L_{q,q'} = \tfrac{1}{2}\sqrt{(j{-}q)(j{+}q{+}1)}\delta_{q+1,q'} + \tfrac{1}{2}\sqrt{(j{+}q)(j{-}q{+}1)}\delta_{q-1,q'}. \tag{24}$$

These matrices are Hermitian, traceless and a basis to represent the algebra su(2). Observe, in particular, the matrix representation of the momentum generator $\mathbf{P}$ in (23); its action $\mathbf{Pf} = \mathbf{f}'$ on a signal $\mathbf{f} = \|f_q\|$ is $-\mathrm{i}$ times a weighted central derivative,

$$f'_q = -\tfrac{1}{2}\mathrm{i}\big(\sqrt{(j{-}q)(j{+}q{+}1)}\,f_{q+1} - \sqrt{(j{+}q)(j{-}q{+}1)}\,f_{q-1}\big). \tag{25}$$

Hence, while in continuous systems momentum generates translations in $q \in \mathsf{R}$, in the su(2) model it generates rotations around the p-axis of figure 3. In the latter, (25) shows that one does not exceed the finite range of positions; for $q = \pm j$ the coefficient of the would-be offending terms $q = \pm(j{+}1)$ is zero.

The Lie exponentials of the su(2) operators (17)–(19) generate the three one-parameter subgroups of SU(2),

$$\mathcal{U}_1(\alpha) = \exp(-\mathrm{i}\alpha\mathcal{Q}), \qquad \mathcal{U}_2(\beta) = \exp(-\mathrm{i}\beta\mathcal{P}), \qquad \mathcal{U}_3(\gamma) = \exp(-\mathrm{i}\gamma\mathcal{L}). \tag{26}$$

In a definite representation, there correspond matrices (22)–(24), which are Hermitian and traceless; it follows that the corresponding groups (26) will be of matrices that are unitary and of unit determinant. Indeed, they can be expressed in closed form as Wigner D^j-matrices [24], and thus provide the linear action of the group SU(2) on the column vector of N-point signals. We incorporate into the algebra the commuting unit operator I (represented by $\mathbf{1}$) that is the generator of overall signal phases $\exp(\mathrm{i}\phi\mathbf{1})$, and which is present in the classification (15) for $A = 0$. We thus have the slightly larger algebra u(2) that generates the group of U(2)-*linear* transformations of N-point signals.

In particular, this slightly larger group includes the fractional *Fourier–Kravchuk* transform, generated by the *number* operator $\mathcal{N} := \mathcal{H} - \frac{1}{2}I = \mathcal{L} + jI$,

$$\mathcal{K}^\alpha := \exp\big(-\mathrm{i}\tfrac{1}{2}\pi\alpha\mathcal{N}\big) = \mathrm{e}^{-\mathrm{i}\frac{1}{2}\pi\alpha j}\exp\big(-\mathrm{i}\tfrac{1}{2}\pi\alpha\mathcal{L}\big), \tag{27}$$

for continuous powers α modulo 4. Closed expressions for the $N \times N$ matrix elements of (26) are given in [13, 14, 17]; they will not be specifically needed here.

5. Weyl-ordered aberrations

Beyond the rigid rotations of the classical sphere, the non-rigid transformations of this manifold are generated by the monomial functions $M^{0,1}_{k,m}$ in (15)–(16). Their corresponding $\mathsf{su}(2)$-quantized operators (17)–(19) will be elements of the universal cover algebra $\overline{\mathsf{su}}(2)$. As in any quantization scheme, there is an inherent ordering ambiguity [25]; we select the *Weyl* ordering scheme: given a classical monomial $q^a p^b \lambda^c$ (a, b, c nonnegative integer powers) and the noncommuting operators $\mathcal{Q}$, $\mathcal{P}$, $\mathcal{L}$, one sums all their $a+b+c$ permutations, and divides by the factorial of this number. The finite quantization of a classical monomial function $q^a p^b \lambda^c$ will be the Weyl-ordered operator $\{\mathcal{Q}^a\mathcal{P}^b\mathcal{L}^c\}_{\mathrm{W}}$, and its representing matrices $\{\mathbf{Q}^a\mathbf{P}^b\mathbf{L}^c\}_{\mathrm{W}}$. A natural basis for $\overline{\mathsf{u}}(2)$ is provided by (15)–(16), which will be denoted by

$$\mathcal{M}^{0,1}_{k,m} := \left\{M^{0,1}_{k,m}(\mathcal{Q},\mathcal{P},\mathcal{L})\right\}_{\mathrm{W}}, \tag{28}$$

and their representing $N \times N$ matrices by boldface.

The Weyl ordering is unique, it distributes with respect to summation, and has the necessary properties that, when the operators are self-adjoint under some inner product (i.e. their representing matrices are Hermitian), then also their Weyl-ordered product is self-adjoint (and the matrices Hermitian); except for the monomials containing even powers of the matrices (22)–(24), their Weyl-ordered products are also traceless. Another important property satisfied only by the Weyl ordering of (15)–(16) is that the commutator of the operators $\mathcal{M}^{0,1}_{k,m} \in \overline{\mathsf{su}}(2)$ with any $\mathcal{M}^{0,1}_{1/2,m} \in \mathsf{u}(2)$, is the same as the Berezin bracket of the corresponding classical monomials. This correspondence holds because of the distributive property of the operators and matrices, which ensures that the sum of all permutations of the elemental factors will again be a sum of all their permutations, except for the one which has been replaced by its commutator. From this follows that for each rank k we have a *multiplet* of aberrations that transform linearly under the group $\mathsf{U}(2)$, with the *same* coefficients as their counterparts on the classical sphere. In particular, the Fourier (–Kravchuk) transform of a monomial (29)–(29) is obtained rotating the sphere in figure 3 around the λ-axis by $\frac{1}{2}\pi$, thus exchanging $p \mapsto q$ and $q \mapsto -p$. These properties are the analogs of similar results for geometric optics [26], where the symplectic algebra $\mathsf{sp}(2,\mathsf{R})$ generates the linear transformations that conserve the aberration orders, and Fourier transformation reflects the aberrations represented in figure 1 across a centered vertical line. However, the commutator between two higher-order elements of $\overline{\mathsf{su}}(2)$ will be generally different between Poisson and Berezin brackets, both in classical and quantum realizations.

Yet, matrix representations of $\mathsf{su}(2)$ cannot lead to faithful matrix representations of $\overline{\mathsf{su}}(2)$ because the number of independent $N \times N$ Hermitian matrices cannot exceed N^2. For concreteness consider the case of $N = 5$-point systems, i.e., $j = 2$. The Lie algebra $\mathsf{u}(5)$ of Hermitian matrices has dimension $5^2 = 25$ while its linear subgroup $\mathsf{u}(2)$ has only $2^2 = 4$, so there should be 21 independent aberration generators to be found and classified. To see which is the highest aberration that can be suffered by signals in such a system, consider the diagonal position matrix $\mathbf{Q}$ in (22) and its successive powers $\mathbf{Q}^n$, starting with $\mathbf{Q}^0 := \mathbf{1}$. The first five powers $n = 0, \ldots, 4$ exhaust the five degrees of freedom of all diagonal matrices, and higher powers will be linear combinations of the previous matrices; since any Hermitian matrix can be diagonalized, this argument applies to any of them. Monomials of order higher than 4 in the $\mathsf{u}(2)$ matrices will not be independent of the 25 5×5 Hermitian matrices provided by (15)–(16).

For our 5-point system thus, the monomials that generate aberrations of orders $0 \leqslant A \leqslant 4$ (integer and half-integer ranks $0 \leqslant k \leqslant 2$), and of the weights m as specified in (15)–(16), can

be organized writing their classical expressions in two 'aberration pyramid' patterns:

$$
\begin{array}{rccccccccc}
M^0_{k,m}(q,p): & & & & & & & & & \\
A=0 & & & & & 1 & & & & k=0 \\
1 & & & & p & & q & & & \tfrac{1}{2} \\
2 & & & p^2 & & pq & & q^2 & & 1 \\
3 & & p^3 & & p^2q & & pq^2 & & q^3 & \tfrac{3}{2} \\
4 & p^4 & & p^3q & & p^2q^2 & & pq^3 & & q^4 \quad 2 \\
m= & 2 & \tfrac{3}{2} & 1 & \tfrac{1}{2} & 0 & -\tfrac{1}{2} & -1 & -\tfrac{3}{2} & -2
\end{array}
\tag{29}
$$

$$
\begin{array}{rccccccc}
M^1_{k,m}(q,p,\lambda): & & & & & & & \\
A=1 & & & & \lambda & & & k=\tfrac{1}{2} \\
2 & & & \lambda p & & \lambda q & & 1 \\
3 & & \lambda p^2 & & \lambda pq & & \lambda q^2 & \tfrac{3}{2} \\
4 & \lambda p^3 & & \lambda p^2q & & \lambda pq^2 & & \lambda q^3 \quad 2 \\
m= & \tfrac{3}{2} & 1 & \tfrac{1}{2} & 0 & -\tfrac{1}{2} & -1 & -\tfrac{3}{2}
\end{array}
\tag{30}
$$

The pyramid of aberrations (29) matches that shown in figure 1, while (30) repeats it with an extra λ that only matters globally on the sphere; the first pyramid has 15 entries while the second has 10, providing the 25 generators of $\mathsf{u}(5)$. These include for $A = 0$ the $\mathsf{u}(1)$ phase, for $A = 1$ the three $\mathsf{su}(2)$-linear generators, and for $A = 2, 3, 4$, the $5, 7, 9$ distinct aberrations.

The general case of $\mathsf{u}(2) \subset \mathsf{u}(N)$, $N = 2j+1$, follows the patterns of (29)–(30) with the entries being $\mathsf{su}(2)$-quantized to the Weyl-ordered matrices $\mathbf{M}^0_{k,m}$ and $\mathbf{M}^1_{k,m}$ from (28). The aberration orders present in $\mathsf{U}(N)$ are thus $0 \leqslant A \leqslant N-1 = 2j$. Again, at the top $A = 0$ are the overall phases, and $A = 1$ contains the three $\mathsf{SU}(2)$-linear transformations. At each aberration order A there will be $2k+1$ matrices $\mathbf{M}^0_{k,m}$ and $2k$ matrices $\mathbf{M}^1_{k,m}$, summing to a total of $2A+1$ distinct aberrations at each order. In the first pyramid there are $\frac{1}{2}N(N+1)$ generators, while in the second there are $\frac{1}{2}N(N-1)$; they sum of course the N^2 generators of $\mathsf{u}(N)$.

We note that aberrations whose generators are represented by purely imaginary matrices will generate—after exponentiation with a $-\mathrm{i}$—real orthogonal matrices; these are elements of the subgroup $\mathsf{SO}(N) \subset \mathsf{U}(N)$, that has $\frac{1}{2}N(N-1)$ parameters; these transformations leave real signals real. Among the $\mathsf{u}(2)$ generator matrices in (22)–(24) only momentum $\mathbf{P}$ is purely imaginary; it follows that among the aberrations in the pyramids (29)–(30), those containing odd powers of p will generate all real orthogonal transformations in N-point signals.

We have already studied several transformations that follow the above classification. We mentioned the Fourier–Kravchuk transform (linear, $A = 1$) generated by $\mathcal{L}$ [17]. A finite Kerr Hamiltonian $\mathcal{L} + \alpha\mathcal{L}^2$ was considered in [27] to study the revivals of coherent states in finite systems; because of (21), the Kerr anomaly $\mathcal{L}^2$ is an aberration of order $A = 2$ with a phase. Also at $A = 2$ is the free Fresnel flight generated by $\frac{1}{2}\mathcal{P}^2 = \frac{1}{2}\mathcal{M}^0_{1,1}$ [18], and Fresnel quadratic-phase lenses are generated by $\mathcal{Q}^2 = \mathcal{M}^0_{1,-1}$. Squeezing (scaling or magnification) is generated by $\{\mathcal{PQ}\}_{\mathrm{W}} = \mathcal{M}^0_{1,0}$. In [19] we also considered $\{\mathcal{PQL}\}_{\mathrm{W}} = \mathcal{M}^1_{3/2,0}$ ($A = 3$), noting that its action matches that of $\mathcal{M}^0_{1,0}$ at the bottom pole of figures 3, but divides the global flow on the phase-space sphere into octants.

6. The unitary aberration group

The factored-product parametrization of canonical transformations in geometric optics (6)–(9), with its nested structure of linear and aberration subgroups of increasing orders [1, chapter 13], plainly suggests the following analog decomposition of the group $\mathsf{U}(N)$ based on a $\mathsf{U}(2)$-linear subgroup. Its elements will be characterized by N^2 parameters forming the list

$$\mathbf{B} \equiv \{\mathbf{B}_A\}_{A=0}^{N-1} \equiv \left\{\left\{\left\{B^0_{k,m}\right\}_{m=-k}^{k}\right\}_{2k=A=0}^{N-1}, \left\{\left\{B^1_{k,m}\right\}_{m=-k}^{k}\right\}_{2k+1=A=1}^{N-1}\right\}, \tag{31}$$

that can also be displayed in the pattern of the monomials (15)–(16). This factored-product order for the group $\mathsf{U}(N)$ will be written as the $N \times N$ representation of

$$\mathcal{U}(\mathbf{B}) = \exp(-\mathrm{i}\mathbf{B}_{N-1} \cdot \mathcal{M}_{N-1}) \times \cdots \times \exp(-\mathrm{i}\mathbf{B}_2 \cdot \mathcal{M}_2) \tag{32}$$

$$\times \exp(-\mathrm{i}\mathbf{B}_1 \cdot \mathcal{M}_1) \times \mathrm{e}^{-\mathrm{i}B_0} \tag{33}$$

$$=: \prod_{A=N-1}^{0\,>} \exp(-\mathrm{i}\mathbf{B}_A \cdot \mathcal{M}_A), \tag{34}$$

$$\mathbf{B}_A \cdot \mathcal{M}_A := \sum_{m=-k}^{k=A/2} B^0_{k,m}\mathcal{M}^0_{k,m} + \sum_{m=-k}^{k=(A-1)/2} B^1_{k,m}\mathcal{M}^1_{k,m}, \tag{35}$$

where as before $\Pi^{>}_A$ is the product of factors with decreasing values of the aberration order A. Although many relevant properties of the factored product (6)–(9) hold for (32)–(35), the composition of parameters under multiplication in $\mathsf{U}(N)$ is of course different from that given in [1, equations (14.71–76)] for Poisson operators.

It is also interesting to examine the range of the parameters $B^{0,1}_{k,m}$ in the list (31). Since the $\mathsf{U}(N)$ group manifold has a finite invariant volume (it is a direct product of complex spheres [28]), the range of its parameters could be expected to be always finite and periodic, as it is for the linear $\mathsf{U}(2)$ subgroup. To this end, consider first the eigenvalues of the spherical aberration matrices $\mathbf{M}^0_{k,k} = \mathbf{P}^{2k}$ $(A = 2k)$; for $N = 2j{+}1$, these are p^{2k} with integer or half-integer $p \in [-j, j]$; the eigenvalues of the matrices exponentiated with $\phi = B^0_{k,k}$ are then $\exp(-\mathrm{i}\phi p^{2k})$. When N is odd (integer j and p's), all these phases return to 1 for $\phi = 2\pi$; but when N is even (half-integer j and p's) this occurs only for $\phi = 2^{2k+1}\pi$. The same holds for the subgroups generated by $\mathbf{Q}^{2k}$ or by $\mathbf{L}^{2k}$ —including the $(k = 1)$ Kerr anomaly [27] with ϕ cyclic modulo 8π (at simple fractions of this period a coherent-state signal will undergo multiple revivals as Schrödinger-cat states). But beyond the previous cases, all other aberrations $|m| < k$, starting with $\{\mathcal{PQ}\}_{\mathrm{W}}$ and $N > 5$ [19], have eigenvalues that seem to be incommensurable. The line ϕ of such one-parameter groups will then be of non-closing Lissajous kind within the finite manifold of $\mathsf{U}(N)$.

The factored-product parametrization (32)–(35) should not be construed as a good global parameterization of $\mathsf{U}(N)$, but as a parametrization of the *neighborhood* of its linear $\mathsf{U}(2)$ subgroup. This is what constitutes an aberration expansion around the paraxial regime; in geometric optics the dimension of the neighborhood is a denumerable infinite, classified by aberration order. In finite systems, the neighborhood is finite-dimensional, and also classified by aberrations as departures from linearity.

In this paper, we are not overly concerned with the compound aberrations that have been computed for geometric optical setups, including corrections for fractional Fourier transformers [1, chapter 15]. Starting with squeezing $\{\mathcal{PQ}\}_{\mathrm{W}}$ we do not have analytic forms for the unitary aberrations, but numerical computation appears to be quite easy. In what follows

we shall concentrate on describing single aberrations, generated by $\mathcal{M}^{\sigma}_{k,m}$ and thus classified by the quantum numbers (k, m, σ). In this context, we can also gloss over the difference between the left-right orders in which operators and matrices act [1, p. 161], by only changing the sign of the parameter. Finally, to show the face of our $\mathsf{U}(N)$ aberrations, we must recall the $\mathsf{su}(2)$ Wigner function to reveal them on the phase-space sphere.

7. The su(2) Wigner function

The phase space provides the scenario to see the aberrations of signals as flows on the surface of a classical sphere (see figure 3). To analyze the one-parameter subgroups of the previous section, we present succinctly the $\mathsf{su}(2)$ Wigner function (see e.g. [15, 27, 29, 30]) and a *sui generis* projection of the sphere onto a rectangle, which we have found convenient in comparing our renderings of finite signals with those of other Wigner functions for continuous signals on the plane. In particular, we emphasize that the finite signals that we treat are understood to be *not* periodic, i.e., there is nothing beyond the signal endpoints.

We first define the $\mathsf{su}(2)$ *Wigner operator* as a manifold of elements in the $\mathsf{SU}(2)$ *group ring* [15, 29], which is a function of the meta-phase space coordinates of position, momentum, and (displaced) energy, $\vec{v} = (q, p, \lambda) \in \mathsf{R}^3$, as

$$\mathcal{W}(\vec{v}) := \int_{\mathrm{SU}(2)} \mathrm{d}g(\vec{w}) \exp \mathrm{i}[w_1(q - \mathcal{Q}) + w_2(p - \mathcal{P}) + w_3(\lambda - \mathcal{L})], \tag{36}$$

where the integration is over the group manifold of $\mathsf{SU}(2)$ with the Haar measure $\mathrm{d}g(\vec{w})$.

We define the *Wigner function* of an N-point signal $\mathbf{f} = \{f_q\}_{q=-j}^{j}$ ($N = 2j+1$, a column vector) as the expectation value of the Wigner operator (36) in that state,

$$W(\mathbf{f}|\vec{v}) := \langle \mathbf{f}|\mathcal{W}(\vec{v})|\mathbf{f}\rangle = \sum_{q,q'} f_q^* W^{(j)}_{q,q'}(\vec{v}) f_{q'}. \tag{37}$$

In the last expression, the Wigner operator is represented by an $N \times N$ *Wigner matrix* $\mathbf{W}^{(j)}(\vec{v}) = \left\| W^{(j)}_{q,q'}(\vec{v}) \right\|$, which is both Hermitian and unitary [15, 29]. Its full expression is given in the appendix, where we also list the radial and axial marginals of this $\mathsf{su}(2)$ Wigner function, and show that one may 'slice' meta-phase space $\vec{v} = (q, p, \lambda) = r\hat{u}(\beta, \gamma)$ at the radius $r = j + \frac{1}{2}$. One thus remains with the Wigner function (37)–(A.2) on the phase-space sphere, with coordinates (β, γ) of colatitude $\beta \in [0, \pi]$ and azimuth $\gamma \in (-\pi, \pi]$ (modulo 2π). On the sphere, and written $W(\mathbf{f}|\beta, \gamma)$, the $\mathsf{su}(2)$ Wigner function (37) becomes equivalent to the phase-space distribution function of Stratonovich [31] and Agarwal [32], as proven in [16]. The Wigner function (37) transforms covariantly under $\mathsf{SU}(2)$, and can be easily extended for density matrices representing mixed states using the trace of its product with the Wigner matrix as usual.

We recall from figure 3 that the colatitude angle β is measured from the q-axis because the position operator $\mathcal{Q}$ in (17) is the one that we chose diagonal; $\beta = 0$ is the '$+q$-pole' (with all γ's equivalent), while the $-\lambda$-axis (the 'bottom pole') is at $\beta = \frac{1}{2}\pi$, and determines the $\gamma = 0$ meridian. Since the interesting region of the phase-space sphere is near the bottom pole, where it is tangent to the phase plane of continuous systems, we find it advantageous to plot $W(\mathbf{f}|\beta, \gamma)$ on the (β, γ) rectangle shown in figure 4. (In [18, 19] instead of a 2:1 rectangle we used a square.)

In figure 5, we show the Wigner function of a rectangle signal; this will serve as a reference for its further transformations. The projection of figure 4 distorts the polar grid of the sphere near to the ends of the β-axis, but near to its center it rather faithfully reproduces the Wigner function of continuous systems. The position marginal of the Wigner function (which

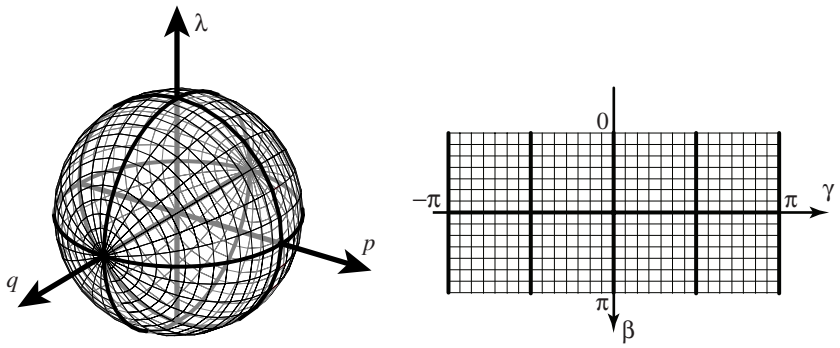

Figure 4. *Left*: polar coordinates on the sphere (β, γ) are referred to the position q-axis so that $\beta = 0$ is the $+q$ direction. *Right*: the (β, γ) plane rectangle, $\beta \in [0, \pi]$, $\gamma \in (-\pi, \pi]$. The bottom pole of the sphere ($\beta = \frac{1}{2}\pi$, $\gamma = 0$) is projected on the center of the rectangle; there, the axis of positions q corresponds to the vertical β-axis, and that of momenta with the horizontal γ-axis. Heavy lines on the sphere mark its intersections with the Cartesian coordinate planes; they are marked similarly on the rectangle. The left and right edges ($\gamma = \pm\pi$) are identified as in a cylinder; the upper edge represents the single point $\beta = 0$ on the $+q$ axis, while the lower edge is the point $\beta = \pi$ on the $-q$ direction.

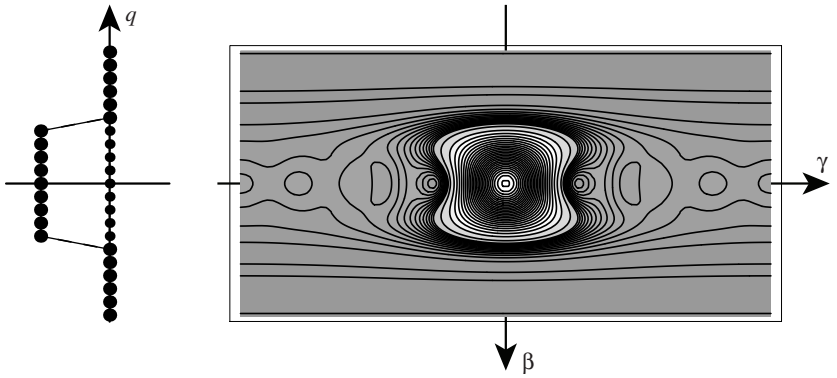

Figure 5. *Left*: centered rectangle signal of $N = 21$ points ($j = 10$), $\mathrm{Rect}_n(q) = 1$ for integer $-n \leqslant q \leqslant n = 4$ and 0 elsewhere. The function 'exists' only on the dots; a continuous line joins them for visibility. *Right*: Wigner function $W(\mathrm{Rect}_4|\beta, \gamma)$ on the sphere, displayed as a contour plot on the (sphere, projected onto the) rectangle indicated in the previous figure. We show the contour lines for the values 0.0, ± 0.0001, ± 0.001, ± 0.01, 0.02, 0.03, ..., 0.15, 0.2, 0.3, ..., 3.0, 3.1.

returns the absolute square of the signal points—see the appendix) is obtained integrating over momentum; this projects the su(2) Wigner function over the rectangles onto their vertical axes.

8. The face of U(N) aberrations

We have chosen the sharp-edged rectangle signal of figure 5 to undergo aberrations, as we did in [18, 19], because its Wigner function has more structure than the smooth low-energy oscillator modes that are often used to illustrate phase-space transformations. The contours in the density plot of the Wigner function are chosen both to highlight the shape of its main peak, and to display the fine structure in the regions where it is less than 5% of the top value π.

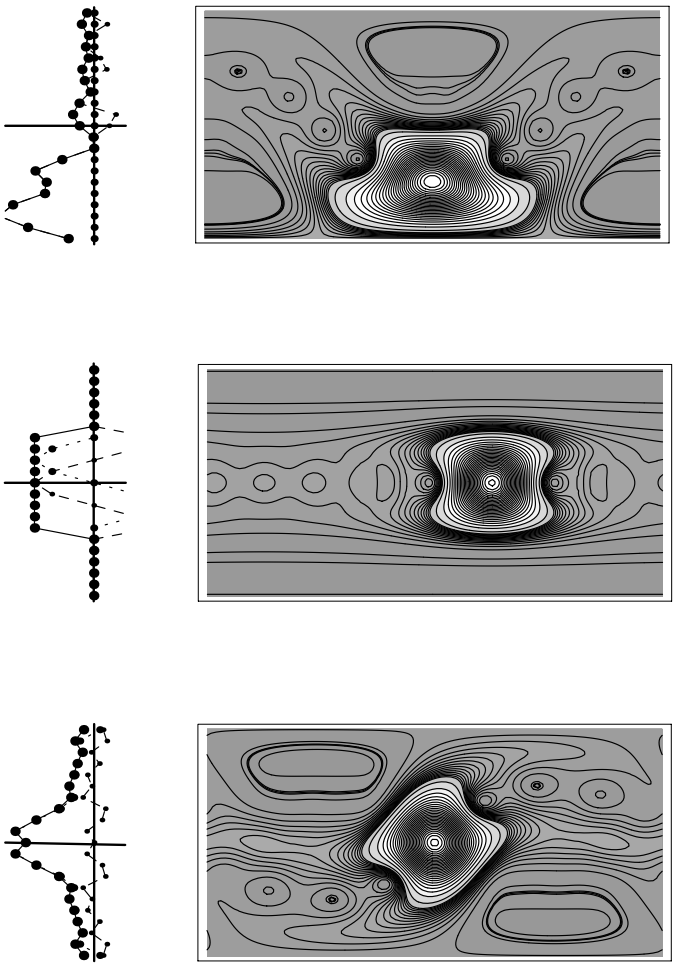

Figure 6. The rectangle signal and Wigner function of the previous figure under SU(2)-linear transformations (26). The real, imaginary, and absolute values of the signals are indicated by dots of increasing size, joined by dashed, dotted, and continuous lines, respectively. All Wigner functions are real and (except for the coherent states, i.e. the finite oscillator ground state rotated by SU(2)) they have small regions of shallow negative values. *Top*: SU(2)-rotation ('translation') in position generated by $p \leftrightarrow \mathbf{P}$, acting through the unitary matrix $\exp(\mathrm{i}\beta\mathbf{P})$, for $\beta = \frac{1}{4}\pi$. *Middle*: SU(2)-translation in momentum (frequency) through $\exp(\mathrm{i}\alpha\mathbf{Q})$, for $\alpha = \frac{1}{4}\pi$. *Bottom*: Fourier-Kravchuk transform (with a phase) generated by $\lambda \leftrightarrow \mathcal{L}$ through $\exp(\mathrm{i}\gamma\pi\mathbf{L})$, for $\gamma = \frac{1}{4}\pi$. Compare the first two phase-space transformations with the second row of figure 1; the third is a 45° rotation of phase space around its center.

In figures 6, we show the three SU(2)-linear transformations generated by p, q, λ in (29)–(30). These are rotations of the sphere that correspond in continuous systems to translations in position, in momentum (see the second row in figure 1), and rotations due to fractional Fourier transformations. As we pointed out above, under these transformations, the Wigner function is rigidly carried along with the rotations of the underlying phase-space sphere; the distortions we see in figures 6 are due to the projection on the (β, γ) rectangle.

Aberrations that distort the surface of the classical sphere will make the Wigner function of a signal wiggle somewhat, as it does in continuous models on the phase-space plane [33].

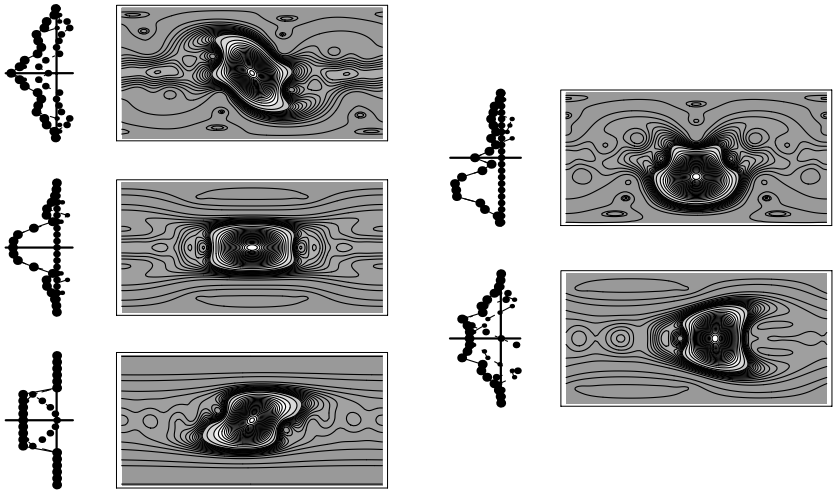

Figure 7. Aberrations of order $A = 2$ in the rectangle signal of figure 5, with coefficient $B_2 = 0.05$. The dots and lines of the signal follow the conventions of the previous figure, and hold for the following ones. *Left column* (top to bottom): aberrations generated by the finite quantization of the classical monomials $p^2 = M^0_{1,1}$, $pq = M^0_{1,0}$, and $q^2 = M^0_{1,-1}$. Compare with the third row in figure 1 of linear transformations in continuous systems. *Right column*: aberrations generated by $\lambda p = M^1_{1,1/2}$ and $\lambda q = M^1_{1,-1/2}$.

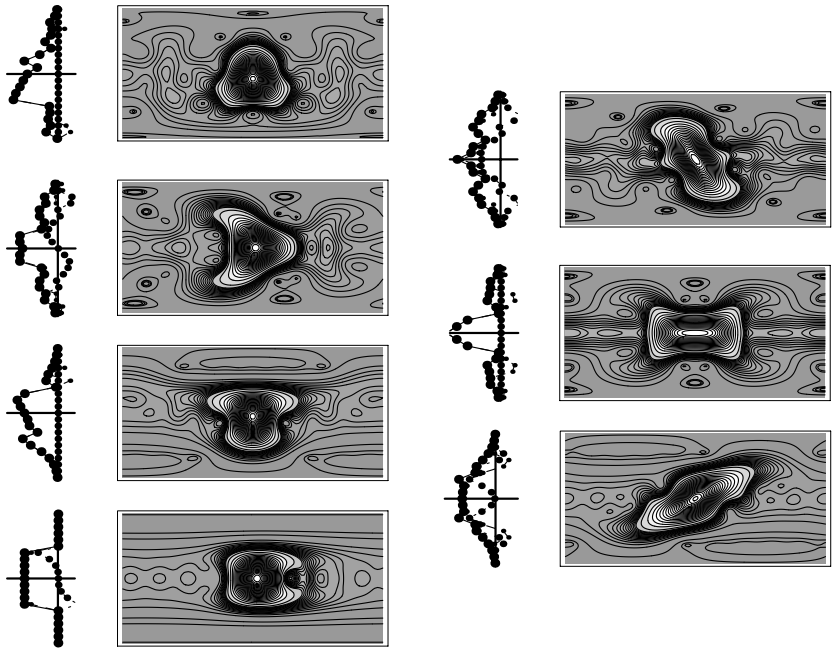

Figure 8. Aberrations of order $A = 3$ in the signal of figure 5, with coefficient $B_3 = 0.01$. *Left column* (top to bottom): aberrations generated by $p^3 = M^0_{3/2,3/2}$, $p^2q = M^0_{3/2,1/2}$, $pq^2 = M^0_{3/2,-1/2}$, and $q^3 = M^0_{3/2,-3/2}$. Compare with the nonlinear maps in the fourth row of figure 1 for continuous systems. *Right column*: aberrations generated by $\lambda p^2 = M^1_{3/2,1}$, $\lambda pq = M^1_{3/2,0}$ and $\lambda q^2 = M^1_{3/2,-1}$.

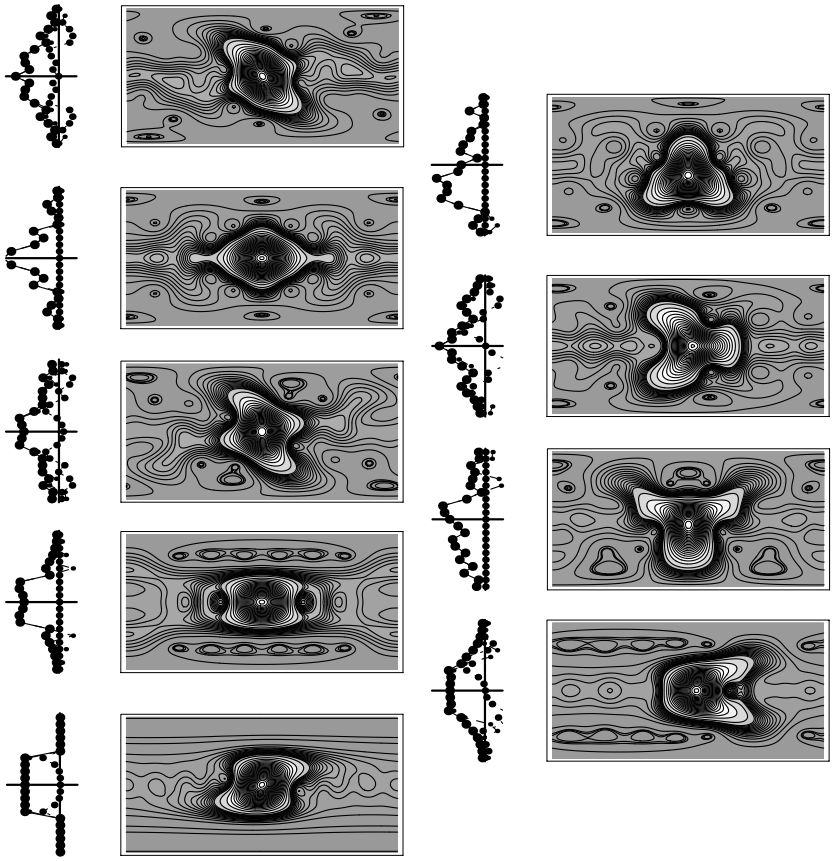

Figure 9. Aberrations of order $A = 4$ in the signal of figure 5, with coefficient $B_4 = 0.002$. *Left column*: aberrations generated by $p^4 = M^0_{2,2}$, $p^3q = M^0_{2,1}$, $p^2q^2 = M^0_{2,0}$, $pq^3 = M^0_{2,-1}$, and $q^4 = M^0_{2,-2}$. Compare with the five aberrations of the bottom row in figure 1 and their flows in figure 2. *Right column*: aberrations generated by $\lambda p^3 = M^1_{2,3/2}$, $\lambda p^2q = M^1_{2,1/2}$, $\lambda pq^2 = M^1_{2,-1/2}$ and $\lambda q^3 = M^1_{2,-3/2}$.

The usefulness of the su(2) Wigner function depends on how recognizable the signal remains after aberration. In figure 7 we show the five aberrations of order $A = 2$, for small values of the parameters, chosen to display the deformation without undue wiggling. Aberration expansions in geometric optics are generally done on the basis of assuming that their parameters are small compared to the linear part of the transformation. As we noted earlier, increasing the parameter values leads to Talbot-like reconstructions for spherical aberrations, or to random partial revivals in other cases. Figure 8 shows the seven aberrations of order $A = 3$, and figure 9 displays the nine aberrations of order $A = 4$. The number of points in the signal was chosen to be $N = 21$ ($j = 10$), so the total number of aberrations these signals can suffer is actually $21^2 - 4 = 437$.

9. Conclusions

One of the purposes of studying finite systems is to model micro-optical devices for parallel signal processing, which have a finite number N of sources and sensors, where the first-

order (paraxial) regime is well understood (for example, the fractional Fourier transform), but aberrations are present that may be corrected [1, chapter 15]. Of course, observing N independent test signals under transformation, one can find the $N \times N$ complex transfer matrix for the system, but its departure from the paraxial design can be quantified only when one has some appropriate basis that allows the aberration coefficients to be extracted order by order. While in geometric optics this 'inverse problem' is unbounded, in finite systems there are aberrations of orders up to $A = N - 1$ only, and to find them (from the transfer matrix of an actual optical system) is a computational task that we see ahead.

It is known that passive optical systems produce canonical transformations of phase space; in geometric optics this means that no rays are lost or gained; in finite systems this means that all information contained in finite complex signals (amplitudes and phases with respect to a basis) will be preserved, i.e., unitarity. In the present finite $\mathsf{su}(2)$ model these requisites are fulfilled by construction, orthonormal bases are natural, and coherent states can be built as in the classical and continuous counterpart models [17]. It remains to be understood exactly how, when $N \to \infty$, unitarity contracts to canonicity. This limit has been probed in the contraction of $\mathsf{su}(2)$ to the Heisenberg–Weyl algebra, in the Hamilton and Newton equations (difference to differential), and in the limit from Kravchuk to Hermite wavefunctions [34], but several aspects in the contraction of the Wigner functions need exploration.

The structure of the $\mathsf{U}(N)$ group as revealed by the factored-product parametrization is new, and certainly appears more complicated than that of Euler angles and phases [28], but it can be managed with symbolic and numerical computation. In particular, the well-known $N \times N$ finite Fourier matrix with its FFT algorithm is an element of the $\mathsf{U}(N)$ group. What are its Euler-angle and factored-product coordinates? How far is it from the Fourier–Kravchuk transform? Two works in this direction are [35, 36].

Much research has gone into producing numerical algorithms for linear canonical transformations of sampled continuous signals [12], to achieve the $\sim N \log_2 N$ efficiency of the FFT. Part of the problem is that the transform kernel is generally a chirping function—which is hard to tame. The finite model has no problem with oscillations, but its linear $\mathsf{U}(2)$ subgroup necessarily involves all N signal points, so its complexity is $\sim N^2$. Thus, the $\mathsf{su}(2)$ model is not computationally fast, but it is exact.

Here, finite quantization based on the Lie algebra $\mathsf{su}(2)$ has led us from geometric optics directly to finite 'N-point optics'. Other Lie algebras that also contract to the Heisenberg–Weyl algebra can be used in a similar fashion. The Euclidean Lie algebra $\mathsf{iso}(2)$ that generates rigid motions of the plane leads to a model whose position space is the set of integers, and momentum space is a circle; the corresponding Wigner function then lives on a phase-space cylinder [37]. Other discrete models based on associative q-algebras have been proposed [38]; there, position space is finite-dimensional —but not equally spaced— and phase space is a revolution spheroïd, but the study of its aberrations has not been pursued yet.

Acknowledgments

I thank G Krötzsch for the figures and discussions on the subject of this paper. Support from the SEP–CONACYT project 44845 *Óptica Matemática* is gratefully acknowledged.

Appendix

To examine the Wigner operator (36) it is convenient to parametrize $g(\vec{w}) \in \mathsf{SU}(2)$ in polar coordinates, with a rotation angle ψ (modulo 2π or 4π) around a unit axis $\hat{u}(\theta, \phi)$ on the

sphere, so $\vec{w} = \psi\hat{u}$. Since $g(\psi\hat{u})^{\nu} = g(\nu\psi\hat{u})$ for any $\nu \in \mathsf{R}$, the unitary action of g on complex N-point signals $\mathbf{f}$, implies that the matrix elements of its Wigner function (37) on the meta-phase space $\vec{v} = (q, p, \lambda)$ can be written as [15, 29]

$$W(\mathbf{f}|\vec{v}) = \int_{\mathrm{SU}(2)} \mathrm{d}g(\vec{w}) \left\langle g\left(-\tfrac{1}{2}\psi\hat{u}\right) : \mathbf{f}\right| \exp(-\mathrm{i}\vec{v}\cdot\vec{w}) \left|g\left(+\tfrac{1}{2}\psi\hat{u}\right) : \mathbf{f}\right\rangle . \tag{A.1}$$

This form is analogous to that of the usual Wigner function [39–41], with $\frac{1}{2}x$-displaced functions to each side and a Fourier transform phase kernel. This form also evinces the covariance of (36) under $\mathsf{su}(2)$ rotations.

Now, writing $\vec{v} = (q, p, \lambda) \in \mathsf{R}^3$ in spherical coordinates $\vec{v}(r, \beta, \gamma)$, we can express the Wigner matrix elements (37) in terms of phases, Wigner *little-d* functions $d^j_{q,q'}(\beta)$ [24] and a diagonal matrix $\overline{W}^{(j)}_{\bar{q}}(r)$ as

$$W^{(j)}_{q,q'}(r, \beta, \gamma) = \mathrm{e}^{-\mathrm{i}(q-q')\gamma} \sum_{\bar{q}=-j}^{j} d^j_{q,\bar{q}}(\beta)\overline{W}^{(j)}_{\bar{q}}(r) d^j_{\bar{q},q'}(-\beta). \tag{A.2}$$

The diagonal matrix is a function only of the radius $r = |\vec{v}|$; it is obtained through a single integral over a finite interval [15],

$$\overline{W}^{(j)}_{\bar{q}}(r) = (-1)^{2j+1}\frac{\pi}{2} \sum_{q=-j}^{j} \int_0^{\pi} \sin\beta \,\mathrm{d}\beta \left|d^j_{\bar{q},q}(\beta)\right|^2 \frac{\sin(2\pi r\cos\beta)}{(r\cos\beta - q)[(r\cos\beta - q)^2 - 1]}. \tag{A.3}$$

Since $d^j_{\bar{q},q}(\beta)$ is a polynomial in trigonometric functions of β, (A.3) may have a closed expression, but we have found it more convenient to compute its $2j+1$ values by numerical integration; this is practical for j up to about 30.

The dependence of the Wigner function (A.1) on the radius r of the meta-phase space is found by calculating the radial marginal over the sphere S_2,

$$M^{(j)}_{\mathrm{rad}}(\mathbf{f}|r) := \int_{\mathrm{S}_2} \mathrm{d}\hat{u}\, W(\mathbf{f}|r\hat{u}) = \|\mathbf{f}\|^2 R_j(r), \tag{A.4}$$

where all radial dependence is in the factor $R_j(r)$. This can be found in terms of sine-integral functions [15],

$$R_j(r) = \frac{4\pi^2}{(2j+1)r}(\mathrm{Si}\,2\pi(r+j) + \mathrm{Si}\,2\pi(r-j) - \mathrm{Si}\,2\pi(r+j+1) - \mathrm{Si}\,2\pi(r-j-1)). \tag{A.5}$$

This function is strongly peaked in the interval $j < r < j+1$, and oscillates with very small values around zero elsewhere [15, figure 2], corresponding to the restriction (21). We have chosen to 'slice' meta-phase space setting the radius to be $r = j + \frac{1}{2}$, so the *Wigner constants* (A.3) need to be calculated only once for each j.

The marginal of position is the projection of the Wigner function onto the q-axis, through integration over $(p, \lambda) \in \mathsf{R}^2$,

$$\begin{aligned} M^{(j)}_{\mathrm{Q}}(\mathbf{f}|q) &:= \int_{\mathrm{R}} \mathrm{d}p \int_{\mathrm{R}} \mathrm{d}\lambda\, W(\mathbf{f}|q, p, \lambda) \\ &= (2\pi)^3 \sum_{q'=-j}^{j} |f_{q'}|^2 \,\mathrm{sinc}\,\pi(q-q'). \end{aligned} \tag{A.6}$$

This function returns the absolute square of the $2j+1$ values of the signal at the positions $\{q\}$ of the system, and sinc-interpolates smoothly between and beyond them.

References

[1] Wolf K B 2004 *Geometric Optics on Phase Space* (Heidelberg: Springer)
[2] Wooters W K 1987 A Wigner-function formulation of finite-state quantum mechanics *Ann. Phys., NY* **176** 1–21
[3] O'Neill J C and Williams W J 1999 Shift covariant time-frequency distributions of discrete signals *IEEE Trans. Signal Process.* **47** 133–46
[4] Klimov A B and Muñoz C 2005 Discrete Wigner function dynamics *J. Opt. B: Quantum Semiclass. Opt.* **7** S588–600
[5] Klimov A B, Muñoz C and Romero J L 2006 Geometrical approach to the discrete Wigner function in prime power dimensions *J. Phys. A: Math. Gen.* **39** 14471–97
[6] Opatrný T 1994 Mean value and uncertainty of optical phase—a simple mechanical analogy *J. Phys. A: Math. Gen.* **27** 7201–8
[7] Opatrný T 1995 Number-phase uncertainty relations *J. Phys. A: Math. Gen.* **28** 6961–75
[8] Forbes G W and Alonso M A 2001 Measures of spread for periodic distributions and the associated uncertainty relations *Am. J. Phys.* **69** 340–7
[9] Forbes G W, Alonso M A and Siegman A E 2003 Uncertainty relations and minimum uncertainty states for the discrete Fourier transform and the Fourier series *J. Phys. A: Math. Gen.* **36** 7027–47
[10] Alonso M A and Bastiaans M J 2004 Mapping-based width measures and uncertainty relations for periodic functions *Signal Process.* **84** 2425–35
[11] Ozaktas H M, Zalevsky Z and Alper Kutay M 2001 *The Fractional Fourier Transform with Applications in Optics and Signal Processing* (Chichester: Wiley)
[12] Koç A, Ozaktas H M, Çandan Ç and Alper Kutay M 2007 Digital computation of linear canonical transforms *IEEE Trans. Signal Process.* at press
[13] Atakishiyev N M and Wolf K B 1997 Fractional Fourier–Kravchuk transform *J. Opt. Soc. Am.* A **14** 1467–77
[14] Atakishiyev N M, Pogosyan G S and Wolf K B 2005 Finite models of the oscillator *Phys. Part. Nucl.* **36** (suppl. 3) 521–55
[15] Atakishiyev N M, Chumakov S M and Wolf K B 1998 Wigner distribution function for finite systems *J. Math. Phys.* **39** 6247–61
[16] Chumakov S M, Klimov A B and Wolf K B 2000 On the connection of two Wigner functions for spin systems *Phys. Rev.* A **61** 034101
[17] Wolf K B and Krötzsch G 2007 Geometry and dynamics in the fractional discrete Fourier transform *J. Opt. Soc. Am.* A **24** 651–8
[18] Wolf K B and Krötzsch G 2007 Geometry and dynamics of the Fresnel transform in finite systems *J. Opt. Soc. Am.* A **24** 2568–77
[19] Wolf K B and Krötzsch G 2007 Geometry and dynamics of squeezing in finite systems *J. Opt. Soc. Am.* A **24** 2871–8
[20] Sánchez-Mondragón J and Wolf K B (ed) 1986 *Lie Methods in Optics (Lecture Notes in Physics* vol 250*)* (Heidelberg: Springer)
[21] Wolf K B 1988 Symmetry-adapted classification of aberrations *J. Opt. Soc. Am.* A **5** 1226–32
[22] Dragt A J 1982 Lie algebraic theory of geometrical optics and optical aberrations *J. Opt. Soc. Am.* **72** 372–9
[23] Dragt A J *Lie Methods for Nonlinear Dynamics with Applications to Accellerator Physics* (University of Maryland), http://www.physics.umd.edu/dsat/dsatliemethods.html
[24] Biedenharn L C and Louck J D 1981 Angular momentum in quantum physics *Encyclopedia of Mathematics and Its Applications* ed G-C Rota (Reading, MA: Addison-Wesley)
[25] Cohen L 1966 Generalized phase-space distribution functions *J. Math. Phys.* **7** 781–6
[26] García-Bullé M, Lassner W and Wolf K B 1986 The metaplectic group within the Heisenberg–Weyl ring *J. Math. Phys.* **27** 29–36
[27] Chumakov S M, Frank A and Wolf K B 1999 Finite Kerr medium: macroscopic quantum superposition states and Wigner functions on the sphere *Phys. Rev.* A **60** 1817–23
[28] Wolf K B 1972 The $U_{n,1}$ and IU_n representation matrix elements *J. Math. Phys.* **13** 1634–8
[29] Ali S T, Atakishiyev N M, Chumakov S M and Wolf K B 2000 The Wigner function for general Lie groups and the wavelet transform *Ann. H. Poincaré* **1** 685–714
[30] Klimov A B 2002 Exact evolution equations for SU(2) quasidistribution functions *J. Math. Phys.* **43** 2202–13
[31] Stratonovich R L 1956 On distributions in representation space *JETP* **31** 1012–20
Stratonovich R L 1957 On distributions in representation space *Sov. Phys.—JETP* **4** 891–8
[32] Agarwal G S 1981 Relation between atomic coherent-state representation, state multipoles, and generalized phase-space distributions *Phys. Rev.* A **24** 2889–2896

[33] Rivera A L, Atakishiyev N M, Chumakov S M and Wolf K B 1997 Evolution under polynomial Hamiltonians in quantum and optical phase spaces *Phys. Rev.* A **55** 876–889
[34] Atakishiyev N M, Pogosyan G S and Wolf K B 2003 Contraction of the finite one-dimensional oscillator *Int. J. Mod. Phys.* A **18** 317–27
[35] Alieva T and Wolf K B 2000 Finite mode analysis through harmonic waveguides *J. Opt. Soc. Am.* A **17** 1482–4
[36] Hakioğ lu T and Wolf K B 2000 The canonical Kravchuk basis for discrete quantum mechanics *J. Phys. A: Math. Gen.* **33** 3313–24
[37] Nieto L M, Atakishiyev N M, Chumakov S M and Wolf K B 1998 Wigner distribution function for Euclidean systems *J. Phys. A: Math. Gen.* **31** 3875–95
[38] Atakishiyev N M, Klimyk A U and Wolf K B 2004 Finite q-oscillator *J. Phys. A: Math. Gen.* **37** 5569–87
[39] Wigner E P 1932 On the quantum correction for thermodynamic equilibrium *Phys. Rev.* **40** 749–759
[40] Bastiaans M J 1978 Wigner distribution function applied to optical signals and systems *Opt. Commun.* **25** 26–30
[41] Hillery M, O'Connel R F, Scully M O and Wigner E P 1984 Distribution functions in physics: fundamentals *Phys. Rep.* **259** 121–67